Analysis of Transmission Characteristics of EBG Structures by Subgridding Unconditionally Stable FETD Method

Yixin Wang[1], Bing Wei[1,*], and Kaihang Fan[2]

[1]School of Physics
Xidian University, Xi'an, 710071, China

[2]School of Information and Communications Engineering
Xi'an Jiaotong University, Xi'an, 710049, China
[*]bwei@xidian.edu.cn

Abstract **–** Subgridding unconditionally-stable finite-element time-domain method based on spatial modes filtering (SSMF-FETD) is combined with the Floquet theorem and used to analyze the transmission characteristics of 2-D dielectric pillar-array electromagnetic bandgap (EBG) structures with cross-section shapes of square and H. The computational stress is effectively reduced by exploiting the periodicity of the EBG structure and subgridding technique. Through the spatial modes filtering (SMF) method, the subgridding FETD (S-FETD) method is developed into the SSMF-FETD with larger time steps and higher computational efficiency. The effect of geometric and electromagnetic parameters on transmission characteristics of EBG structures are analyzed and compared in detail, the conclusions are as follows: the optimal filling ratio of the dielectric square-pillar EBG structure is 0.5, the composite H-pillar EBG structure has multiple bandgaps and can effectively save metal materials while satisfying the design requirements. The effect of electromagnetic parameters can be uniformly analyzed from the perspective of the average relative permittivity; with its increase, the central frequency of the bandgap becomes lower. It should be noted that the bandgap distribution and variation of composite H-pillar EBG structure are related to how its dielectric parameters change and combine. The results can serve as a reference for similar structures design.

Index Terms **–** electromagnetic bandgap (EBG), finite-element time-domain (FETD), Floquet theorem, spatial modes filtering (SMF), subgridding technique.

I. INTRODUCTION

Electromagnetic bandgap (EBG) is a type of electromagnetic structure that can prevent electromagnetic wave propagation in specific frequency ranges [1]. Similar to the photonic band gap (PBG) structures in the optical band, EBG structures can be directly composed of various dielectrics, metals, or other hybrid materials which are arranged periodically in a vacuum, or implanted into the base material. Due to the obvious bandgap characteristic, EBG structures have been applied in many fields in recent years [2, 3]. It can be used to design microwave devices such as broad band-stop filters and high-Q resonators [4, 5], improve antenna performance [6–8] or design multi-frequency antennas [9, 10], increase the efficiency and output power of power amplifiers and be used as frequency selection surfaces[11, 12], etc. For the numerical simulation of 2-D EBG structures with regular geometric shapes, the finite-difference time-domain (FDTD) method [13–15] is used more frequently than the finite-element time-domain (FETD) method [16, 17]. The principle of FDTD is simple and it's easy to implement by programming. At the same time, FETD is suitable for dealing with complex media [18] and its discretization schemes are more flexible and convenient. However, if the EBG structure contains complex and fine structures, the space step size will be very small to capture them accurately when discretizing the computational domain, which will increase the number of grids and memory demand by a considerable amount. At the same time, both FDTD and FETD are limited by the stability condition [19]. The time step is restricted by the minimum space step and has to be very small, which leads to long calculation time and low efficiency. These present a great challenge to the traditional FDTD and FETD method.

Recently, the spatial modes filtering (SMF) method has been proposed and introduced to FDTD and FETD [20–22] to break through the stability condition by filtering out the spatial modes that are unstable under the given larger time step from the numerical system, which substantially improves the computation efficiency. Later, the SMF-FETD method based on subgridding technique (SSMF-FETD) is proposed in [23].

Submitted On: July 01, 2022
Accepted On: November 09, 2022

https://doi.org/10.13052/2022.ACES.J.370901

The use of subgridding technique can not only ensure the discretization quality required by fine structures but also avoid over-division in the region without fine structures. At present, the researches on EBG structures mainly focus on the multifunctional design of metal patch EBG structures and their applications in microstrip structures [2–5, 14–16], etc. However, there are insufficient research on the effect on electromagnetic characteristics of EBG structures composed of multiple material pillars caused by cross-section shapes, combination ways, and electromagnetic parameters.

In this paper, the SSMF-FETD method [23], which has natural advantages in simulating EBG structures, is used to conduct a numerical analysis on a dielectric square-pillar EBG structure and a composite H- pillar EBG structure. In the spatial domain, due to the regular geometric shape of EBG structures, discretizing the computational domain with rectangular grids is enough to ensure modeling accuracy. Using refined rectangular grids to capture the fine structures in EBG structure not only increases the discrete flexibility but also avoids creating excessively unnecessary unknowns in other regions. Besides, the computational domain is reduced by introducing the Floquet periodic boundary condition. In the time domain, the time step of FETD is effectively expanded through the SMF method, thus the time domain iteration pressure is reduced, and the calculation time is shortened.

Through analyzing the influence of geometric and electromagnetic parameters on the transmission characteristics of EBG structures, it can be seen that the optimal filling ratio of the dielectric square-pillar EBG structure is 0.5, the composite H-pillar EBG structure has multiple bandgaps and can effectively save metal materials on the basis of satisfying design requirement. The influence of electromagnetic parameters on EBG structures can be uniformly analyzed from the perspective of the average relative permittivity as: with its increase, the central frequency of bandgap becomes lower. It should be noted that the bandgap distribution and variation of the composite H-pillar EBG structure are related to how its dielectric parameters at the grooves on both sides change and combine.

II. CALCULATION MODEL AND NUMERICAL METHOD

A. Calculation model of EBG Structure

A 2-D EBG structure composed of dielectric square pillars periodically arranged in a vacuum is shown in Fig. 1 (a). There are N layers of pillars in the x-direction and infinite layers in the y-direction. The cross-section side length of the pillar is a, the relative permittivity is ε_r, and the periodic length of EBG unit is r.

The relevant boundary condition settings of a calculation periodic unit T when N=6 are shown in Fig. 1 (b). The absorbing boundary condition (ABC) is set in the x-direction, and the Floquet theorem $f(x,y+T,t) = f(x,y,t))$ can be used to introduce the periodic boundary condition (PBC) and simplify the calculation because there are infinite layers in the y-direction. The planar differential Gaussian pulse is set at the position of the excitation source. The line integral of the transmitted fields is obtained at the observing position, as E_{t1} for the presence of dielectric pillars and E_{t0} for the absence. The transmission coefficient of the EBG structure is calculated by the ratio of E_{t1} and E_{t0} after Fourier transform as:

$$\text{Transmissioncoefficient} = \frac{\text{FFT}(E_{t1})}{\text{FFT}(E_{t0})}.$$

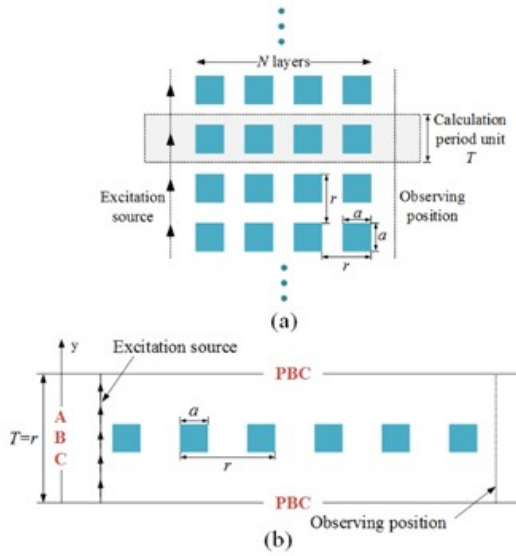

Fig. 1. (a) The 2-D dielectric square-pillar EBG structure. (b) Boundary condition settings of a calculation periodic unit T.

B. Numerical method

The traditional FETD discretization scheme generally requires conforming grids to divide the whole domain [24], and the scale is Δ usually determined by the incident wave as:

$$\Delta \le \frac{\lambda}{10} = \frac{\lambda_0}{10\sqrt{\varepsilon_r \mu_r}},$$

where ε_r and μ_r are the electromagnetic parameters of the target domain, λ and λ_0 are the wavelength of the incident wave in the target domain and in a vacuum respectively. For the 2-D EBG structure model shown in Fig. 1, the space step required by dielectric pillars is obviously smaller than that required by the vacuum background, which would lead to an unnecessarily over-fine

discretization of the vacuum domain. In this scenario, the introduction of the subgridding technique can create a more rational discretization scheme with fewer spatial elements in the computational domain.

As shown in Fig. 2, suppose the dielectric pillar is uniformly divided by fine grids of scale l_f and the remaining vacuum domain is divided by coarse grids of scale l_c. The coarse-to-fine ratio is defined as $Ratio = \frac{l_c}{l_f}$. Dealing with the discontinuous field values caused by the different number of edges at the coarse-fine boundary is the core of the subgridding FETD (S-FETD). Taking the edges at the upper coarse-fine boundary as an example, the electric fields are denoted as $E_5 - E_9$ at the fine boundary, as E_1 at the coarse boundary in Fig. 2. The electric fields at the coarse-fine boundary have to be interpolated [23], the $E_5 - E_9$ are respectively equal to $\frac{1}{Ratio}$ of E_1, so the continuity of the fields is ensured and repeated calculation is avoided.

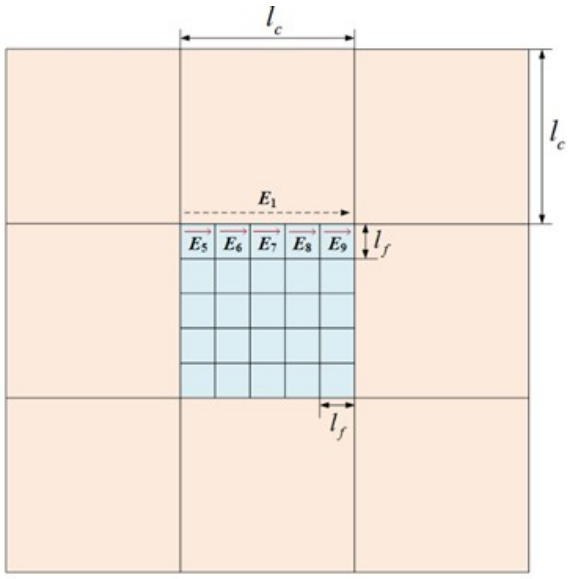

Fig. 2. Electric fields at the upper coarse-fine boundary of subgridding element.

The actual computation starts with processing the edge basis functions which are associated with edge lengths. The fine-edge basis functions at the boundary can be directly written as the 1/Ratio of the coarse-edge basis function [23]. Subsequently, the coarse and fine regions are respectively constructed into a system matrix, where the coarse region is in the order of first the inside edges and then the boundary edges, and the fine region is in the order of first the boundary edges and then the inside edges. After completion, the two system matrices are combined into a complete system matrix T and S in the order of first coarse region and then fine region. However, the T and S matrix both contain the related items that represent the coupling relationship between the coarse boundary edges. For ensuring the continuity of the fields, it is necessary to delete them and only retain their corresponding fine-edge-related items in the calculation [23]. Then the S-FETD system equation can be obtained as follows [23]:

$$T_{new}\frac{d^2 e_{new}}{dt^2} + S_{new} e_{new} = h_{new},$$

where T_{new} and S_{new} are the new system mass matrix and stiffness matrix without the items that relate to the coarse boundary edges, e_{new} is the correlation coefficient vector of the edge basis function, h_{new} is the excitation vector.

Although the S-FETD method can reduce the number of grids, its time step is still limited by the stability condition. Since the system matrices established after the introduction of subgridding technique in the finite-element framework still maintain the characteristics of symmetric positive definite or symmetric semi-positive definite [23], the SMF method can be directly applied to S-FETD to break through the limitation of the time step Δ_t by the minimum spatial step. By solving the generalized eigenvalue problem of the system, and then excluding the unstable eigenmodes from the basic numerical system, the simulation stability under the given large time step can be guaranteed [22]. The unstable modes are required to satisfy [22]:

$$\lambda_i^2 \geq \frac{4}{\Delta t^2},$$

where λ_i^2 is the ith eigenvalue of the system matrix, and the column vectors of matrix Φ_h are the eigenvectors of unstable modes. Then the S-FETD can be developed into SSMF-FETD with a new system without unstable modes through simple modification, and the system matrix equation is changed into [23]:

$$\mathrm{T}_{new}\frac{d^2 e_{new}}{dt^2} + \mathrm{S}_{new}\left(\mathrm{I} - \Phi_h \Phi_h^T \mathrm{T}_{new}\right) e_{new} = h_{new}.$$

III. TRANSMISSION CHARACTERISTIC ANALYSIS OF THE SQUARE-PILLAR EBG STRUCTURE

In this section, the efficiency and accuracy of the SSMF-FETD method are verified by calculating the transmission coefficient of the square-pillar EBG structure. Meanwhile, the effect of geometric and electromagnetic parameters on its transmission characteristics is analyzed.

A. Efficiency and accuracy verification of SSMF-FETD

The parameters of the dielectric square-pillar are as follows: cross-section side length is a=0.01 m, periodic length of EBG unit is r=0.02 m, relative permittivity is $\varepsilon_r = 14$. The coarse and fine grids are of scale $l_f = 0.0004$ m and $l_c = 0.002$ m. The pulse width is $\tau = 2 \times 10^{-10}$s and the pulse peak value is at $t_0 = \tau$.

Figure 3 shows the transmission coefficient of the 2-D dielectric square-pillar EBG structure obtained from FETD, S-FETD, and SSMF-FETD respectively, and the calculation results are in good agreement. It can be seen from Table 1 that compared with the FETD which has 63175 unknowns, the S-FETD effectively reduces the number of unknowns by nearly 84% through the subgridding technique. On this basis, the SSMF-FETD adopts the SMF method to expand the time step and reduces the time occupied by time marching. Although it takes some time and memory to solve the generalized eigenvalue problem, SSMF-FETD still improves the calculation efficiency overall. The results show that the SSMF-FETD method is efficient and accurate in EBG structure simulation.

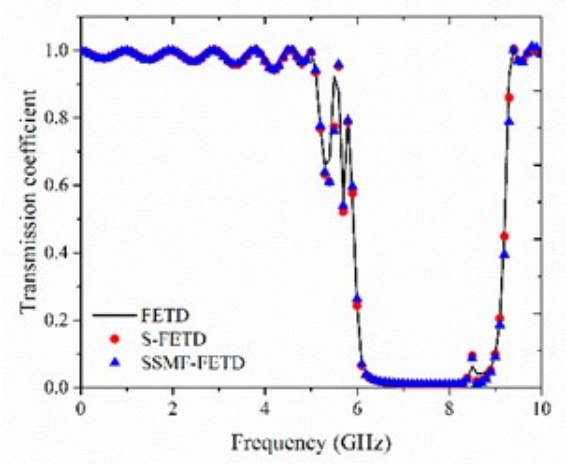

Fig. 3. Transmission coefficient of EBG structure obtained from different methods.

Table 1: Simulation parameters of different methods

Methods	Size of the System Matrix	Time Step (s)	Time for Eigenvalue Analysis (s)	Time for Time Marching (s)	Memory (MB)
FETD	63175	5×10^{-13}	Null	1786.60	72.79
S-FETD	10075	5×10^{-13}	Null	311.84	18.54
SSMF-FETD	10075	3.25×10^{-12}	33.18	161.03	4655.00

B. Effect of geometric parameters

Figures 4 and 5 respectively show the effect of the side length a and periodic length r on transmission coefficient when $\varepsilon_r = 14$. When r = 0.020 m, as a increases, the central frequency of bandgap gradually becomes lower, the bandwidth increases at first and then decreases, and reaches the maximum when a=0.010 m. When a=0.010 m, as r increases, the central frequency of bandgap becomes lower, the bandwidth increases at first and then decreases, and reaches the maximum when r=0.020m. As r increases continuously, the EBG structure gradually exhibits dual-band characteristics. Through Fig. 4 and Fig. 5, it can be verified that for such a square-pillar EBG structure, the bandgap width is the widest when the filling ratio ($\frac{a}{r}$) is 0.5.

C. Effect of electromagnetic parameters

The effect of the relative permittivity ε_r of the dielectric pillar on the EBG structure is shown in Fig. 6, where f_1 and f_h denote the lowest and highest frequency of the bandgap satisfied $S_{21} < -20dB$, f_0 and BW denote the central frequency and bandwidth. It can be seen that as ε_r increases, the central frequency of the bandgap becomes lower and the bandwidth becomes narrower.

Suppose there is a more complex and practical composite dielectric square-pillar EBG structure that contains two different dielectric materials on the basis of the above structure. A dielectric square pillar with side length b and dielectric constant ε_{r2} is surrounded by a layer of dielectric material with ε_{r3} outside. The structural parameters of the composite dielectric square-pillar EBG are still a=0.01 m and r=0.02 m. The coarse grids shown in Fig. 7 (a) cannot accurately describe the pillar. However, the subgridding discretization scheme shown in Fig. 7 (b) can satisfy the requirements of geometric and dielectric parameters on space step at the same time.

When a and r remain unchanged, the effect of changing b, or the relative permittivity ε_{r2}, ε_{r3} on transmission characteristics of the EBG structure, can be attributed to the change of the average relative permittivity ε_r' of the composite dielectric pillar. It is clear that ε_r' is a function of ε_{r2}, ε_{r3} and dielectric-pillar area as follow:

$$\varepsilon_r' = \frac{S_b}{S_a}(\varepsilon_{r2} - \varepsilon_{r3}) + \varepsilon_{r3},$$

where $S_b = b^2$ is the internal area, $S_a = a^2$ is the overall area of the composite pillar.

The change of average relative permittivity ε_r' caused by the electromagnetic parameters (shown in Fig. 8 (a) and Fig. 8 (b)) and geometric parameters (shown in Fig. 8 (c) and Fig. 8 (d)) can affect the central frequency and bandwidth of the composite square-pillar EBG structure. It can be seen that ε_r' can be increased by increasing $\varepsilon_{r2}, \varepsilon_{r3}$ or the filling area with the larger relative permittivity. In the four different cases shown in Fig. 8, as ε_r' increases, the central frequency of the bandgap becomes lower and the bandwidth becomes narrower. This rule is also applicable to the composite square-pillar EBG structure has more layers of dielectric materials.

In fact, ε_r of the single-dielectric square pillar shown in Fig. 1 is equivalent to ε_r'. Then, whether it is a single-dielectric or multi-dielectric square-pillar EBG structure, by increasing or decreasing the ε_r', the central frequency of the bandgap can become lower or higher, also the bandwidth can become wider or narrower.

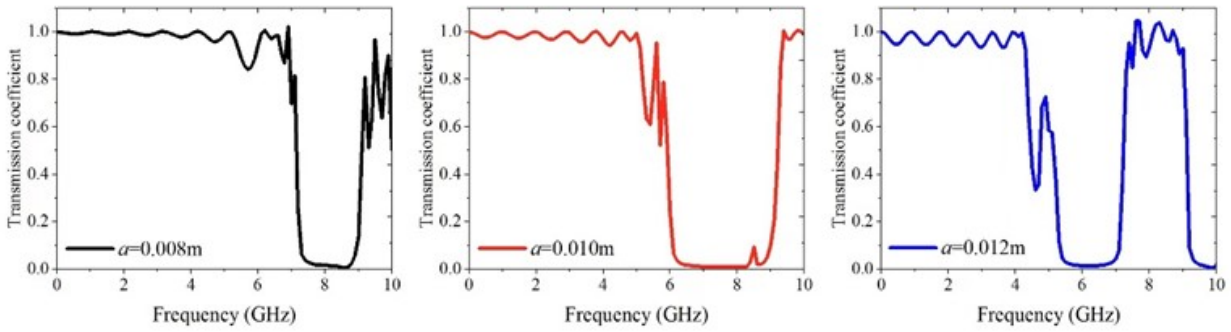

Fig. 4. Effect of a on transmission coefficient when r=0.020m.

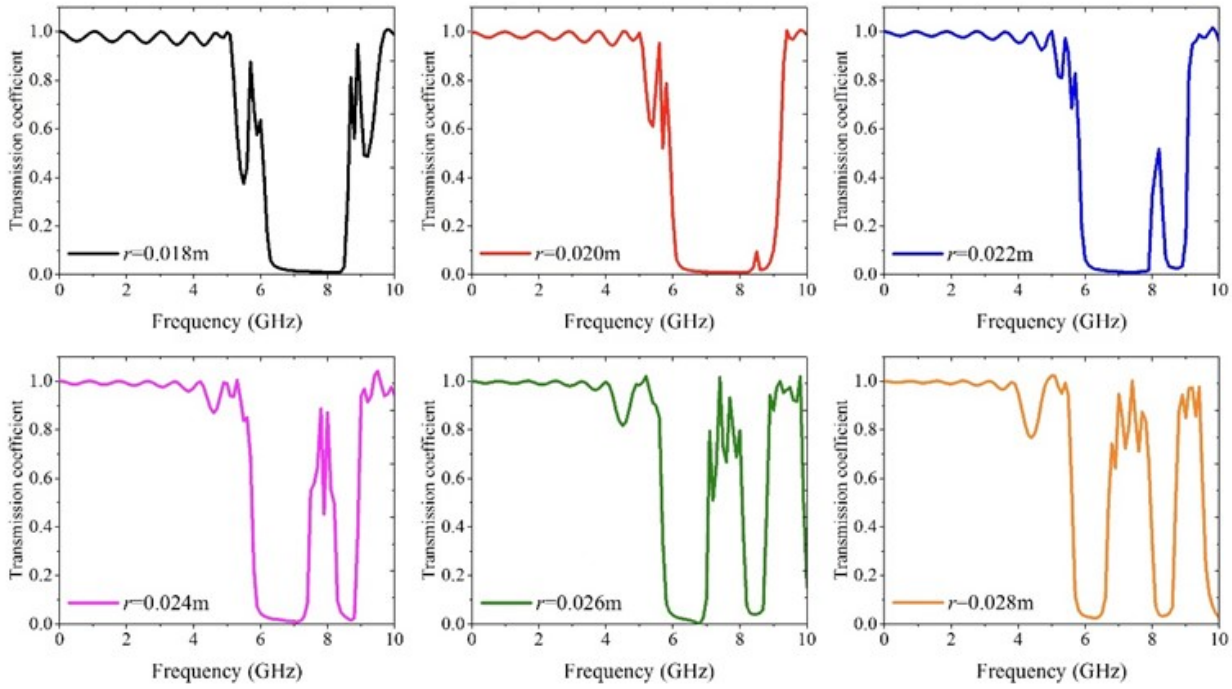

Fig. 5. Effect of r on transmission coefficient when a=0.010 m.

The effects of the geometric and electromagnetic parameters on the transmission coefficient of the dielectric square-pillar EBG structure are analyzed in this section. It is verified that the optimal filling ratio of the square-pillar EBG structure is 0.5. Also, as the average relative permittivity increases, the central frequency of the bandgap becomes lower and the bandwidth becomes narrower.

IV. TRANSMISSION CHARACTERISTIC ANALYSIS OF THE COMPOSITE H-PILLAR EBG STRUCTURE

In this section, a composite H-pillar EBG structure that can satisfy the design requirements and save metal materials is proposed. The effects of geometric and electromagnetic parameters on transmission characteristics are analyzed respectively by adjusting the size and relative permittivity of the grooves on both sides of the H-pillar.

A. Design requirements

The periodic arrangement of metal materials or hybrid materials in a vacuum can also produce EBG structures. The excitation source parameters are $\tau = 8 \times 10^{-10}s$ and $t_0 = \tau$, under this situation, it is required to design an EBG structure whose frequency range of bandgap satisfied $S_{21} < -20dB$ is not less than 1.28∼1.50 GHz. If the square pillar shown in Fig. 1 is

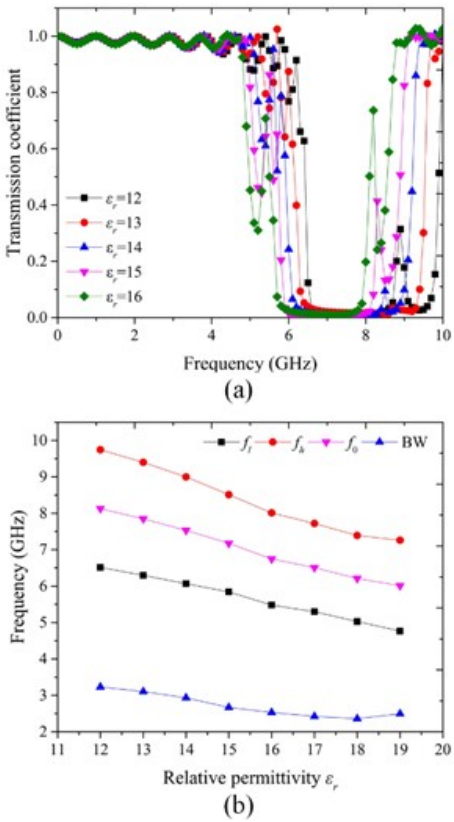

Fig. 6. Effect of relative permittivity ε_r (a) on transmission coefficient, (b) on central frequency and bandwidth.

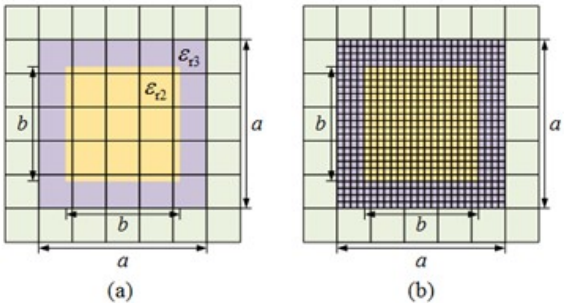

Fig. 7. Mesh model of the composite dielectric square pillar. (a) The coarse mesh scheme. (b) The subgridding scheme.

made of metal, the bandgap of the metal square-pillar EBG structure with a = 0.04 m and r = 0.10 m can satisfy the design requirement.

However, it will be extremely expensive to design with precious metal materials, which are scarce in the Earth's crust and difficult to explore, mine, and refine. For the purpose of saving materials and reducing costs, parts of the metal square pillar can be symmetrically hollowed out and filled with dielectric materials to form a composite H-pillar, and then a composite H-pillar EBG structure. The length of the groove in the H-pillar is p, the width is q, and the dielectric parameters at the grooves on both sides are ε_{r1} and ε_{r2} respectively. As shown in Fig. 9 (a), the spatial grids with a scale of $l_c = 0.01$ m determined by the incident wave cannot describe the structure accurately, but it can be solved by using the fine grids $l_f = 0.002$ m to refine the 4×4 coarse grids occupied by the composite H-pillar as Fig. 9 (b). For simplifying the calculation, the metal material is regarded as the perfect electric conductor (PEC).

Figure 10 shows the transmission characteristics (S_{21} parameter) of the metal square-pillar EBG structure and composite H-pillar EBG structures without dielectric material ($\varepsilon_{r1} = \varepsilon_{r2} = 1$). The geometric parameters of the 'H-pillar_1' case are p = 0.016 m and q = 0.008 m, and the 'H-pillar_2' case corresponds to p = 0.010 m and q = 0.036 m. Compared with the square-pillar case, the bandwidth of the two H-pillar EBG structures are slightly increased, and the performance is improved. Table 2 shows the detailed bandgap parameters of these three EBG structures. It can be seen that the design requirements are satisfied, indicating that the H-pillar EBG structure can save materials effectively while maintaining the performance of the metal square-pillar EBG structure. The cross-sectional area filled with metal materials has been reduced by 16% and 45% respectively, which is of great significance for saving precious metal materials and costs.

The composite H-pillars without dielectric material in both grooves actually construct a pure metal EBG structure. However, when grooves are filled with dielectric materials, the H-pillar EBG structure becomes a multi-band electromagnetic structure, which exhibits the double-bandgap or triple-bandgap characteristic. The first bandgap of them still satisfies the design requirement of 1.28∼1.50 GHz, but the propagation of electromagnetic waves in a certain high-frequency range is also prevented because of the second or third bandgap. It is significant for the design of multi-frequency and frequency-selective working devices.

B. Effect of geometric parameters

Figure 11 (a) and Fig. 11 (b) respectively show the effect of p and q on the transmission characteristics (S_{21} parameter) when $\varepsilon_{r1} = \varepsilon_{r2} = 4$. The EBG structure presents the dual-band characteristic at this time. When q = 0.008 m, as p increases from 0.014 m to 0.018 m, the performance of the first bandgap is slightly improved, the central frequency of the second bandgap becomes lower, and its bandwidth becomes narrower. When p = 0.016 m, as q increases from 0.004 m to 0.012 m, the performance of the first bandgap is improved, the cen-

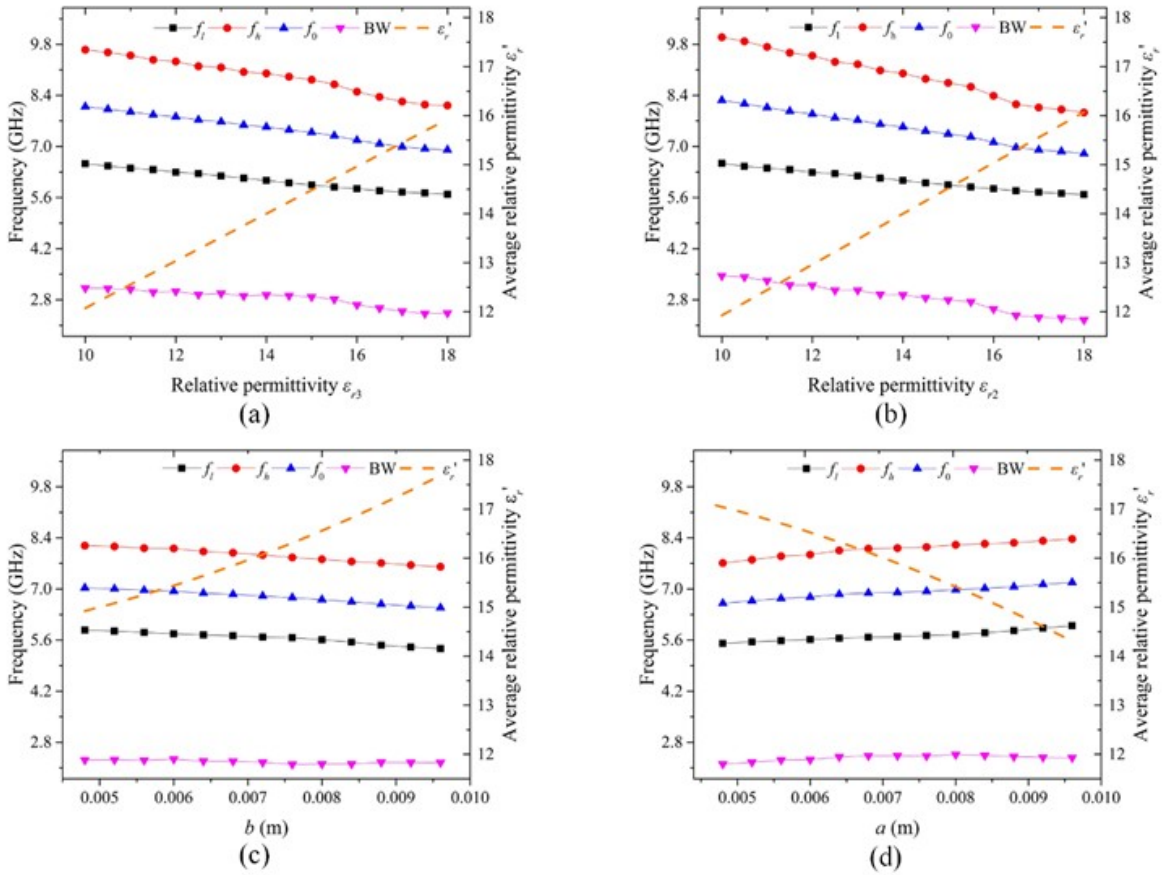

Fig. 8. Effect of average relative permittivity on the central frequency and bandwidth of bandgap. (a) Caused by ε_{r3} (When $b = 0.0072\ m,\ \varepsilon_{r2} = 14$). (b) Caused by ε_{r2} (When $b = 0.0072\ m,\ \varepsilon_{r3} = 14$). (c) Caused by b (When $\varepsilon_{r2} = 18,\ \varepsilon_{r3} = 14$). (d) Caused by b (When $\varepsilon_{r2} = 14,\ \varepsilon_{r3} = 18$).

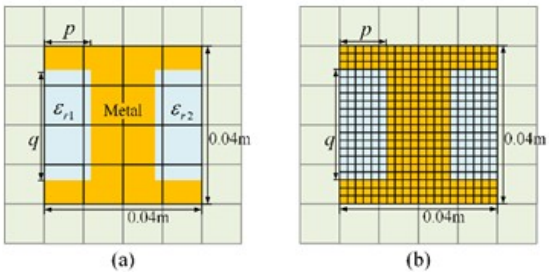

Fig. 9. Mesh model of the composite H-pillar. (a) The coarse mesh scheme. (b) The subgridding scheme.

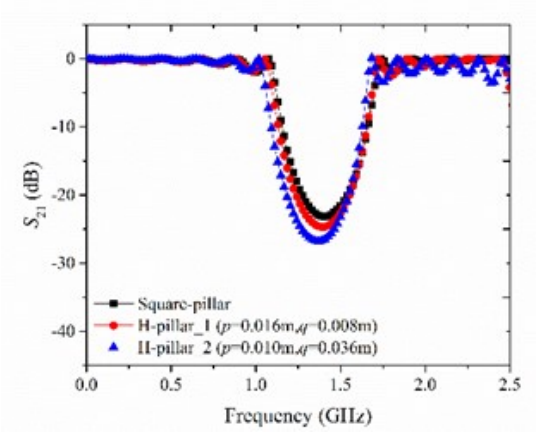

Fig. 10. Transmission characteristics (S_{21} parameter) of metal EBG structures with different cross-section shapes.

tral frequency becomes lower, and the bandwidth is basically unchanged; the performance of the second bandgap is improved, and its central frequency becomes lower while its bandwidth is obviously increased, meanwhile the pass-band between the two bandgaps becomes narrower.

Table 3 further shows the effect of q on central frequency and bandwidth when p = 0.016 m, where the suffixes 1-3 indicate the serial number of bandgaps, and the BW-total denotes the sum of all bandwidths. It

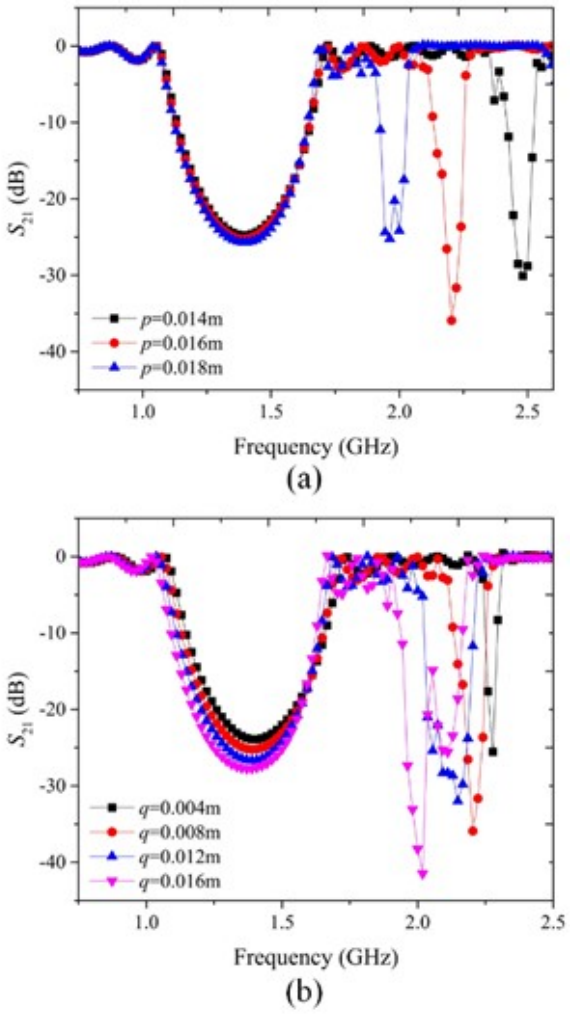

Fig. 11. The effect of geometric parameters on transmission characteristics. (a) Caused by p. (b) Caused by q.

Table 2: Bandgap parameters of metal EBG structures with different cross-section shapes

	Requirements	Square-pillar	H-pillar_1	H-pillar_2
f_l(GHz)	≤ 1.28	1.27451	1.23632	1.18103
f_h(GHz)	≥ 1.50	1.53956	1.55438	1.54754

can be seen that the EBG structure has three bandgaps when $q \geq 0.016$ m. As q increases, the central frequency of the first bandgap becomes lower and its bandwidth becomes narrower, but the design requirements are still satisfied; the central frequency and bandwidth of the second bandgap become lower and wider respectively; the central frequency and bandwidth of the third bandgap become higher and wider respectively. Overall, as q increases, the total bandwidth of bandgaps increases.

Table 3: The effect of q on central frequency and bandwidth of bandgaps

q/m	f_0-1 (GHz)	BW-1 (GHz)	f_0-2 (GHz)	BW-2 (GHz)	f_0-3 (GHz)	BW-3 (GHz)	BW-total (GHz)
0.016	1.370	0.392	1.997	0.085	2.105	0.074	0.551
0.020	1.355	0.405	1.920	0.091	2.072	0.075	0.572
0.024	1.343	0.415	1.904	0.113	2.071	0.079	0.607
0.028	1.329	0.405	1.908	0.134	2.100	0.098	0.636
0.032	1.317	0.409	1.892	0.149	2.101	0.103	0.660
0.036	1.302	0.404	1.869	0.170	2.106	0.099	0.673

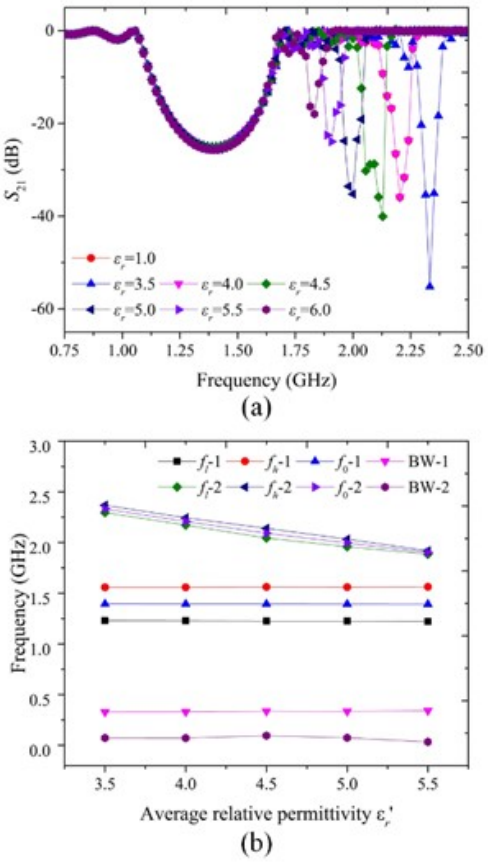

Fig. 12. Effect of ε_r' on transmission characteristics when $\varepsilon_{r1} = \varepsilon_{r2}$. (a) S_{21} parameter. (b) Central frequency and bandwidth.

By analyzing the effect of geometric parameters on transmission characteristics of the composite H-pillar EBG structure, it can be known that adjusting the size of the H-pillar grooves can control the generation of the second, and third bandgap and the movement of their central frequencies.

C. Effect of electromagnetic parameters

The average relative permittivity of the dielectric regions in the composite H-pillar is $\varepsilon_r' = (\varepsilon_{r1} + \varepsilon_{r2})/2$ and the geometric parameters of H-pillar are p = 0.016 m and q = 0.008 m. Figure 12 shows the effect of ε_r' on

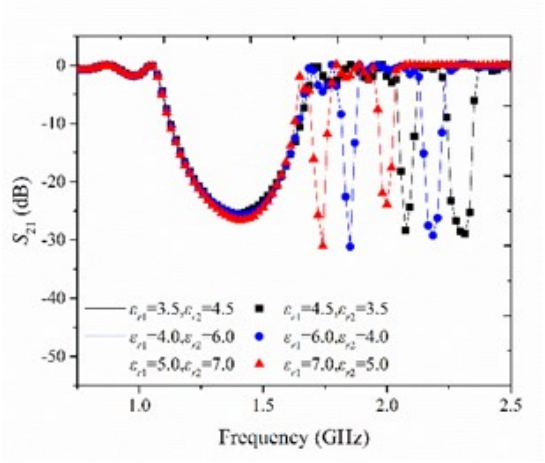

Fig. 13. Effect of ε_r' on transmission characteristics when $\varepsilon_{r1} \neq \varepsilon_{r2}$.

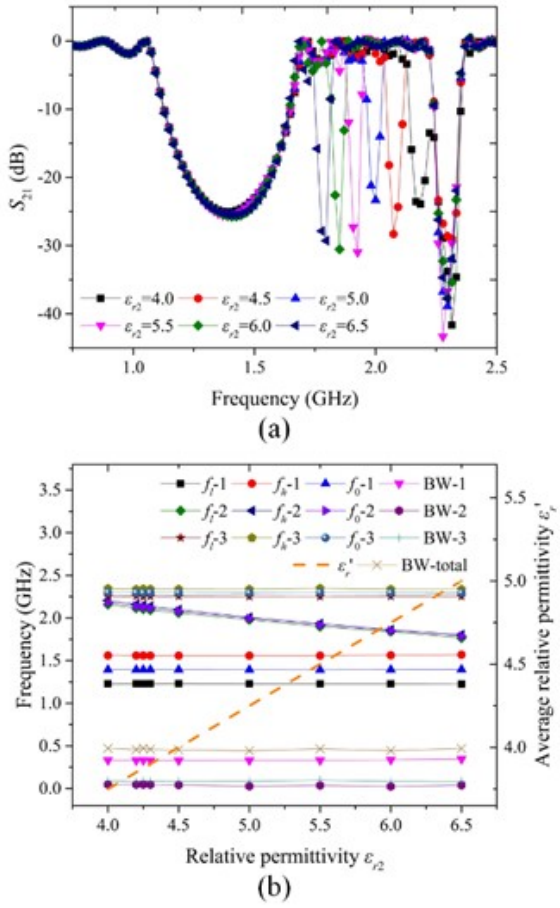

Fig. 14. Effect of ε_r' on transmission characteristics when ε_{r1} is constant. (a) S_{21} parameter. (b) Central frequency and bandwidth.

transmission characteristics when $\varepsilon_{r1} = \varepsilon_{r2}$. As ε_r' increases from 3.5 to 6.0, the first bandgap remains practically unchanged, the central frequency of the second bandgap becomes lower and its performance decreases, and the widest bandwidth appears when $\varepsilon_r' = 4.5$.

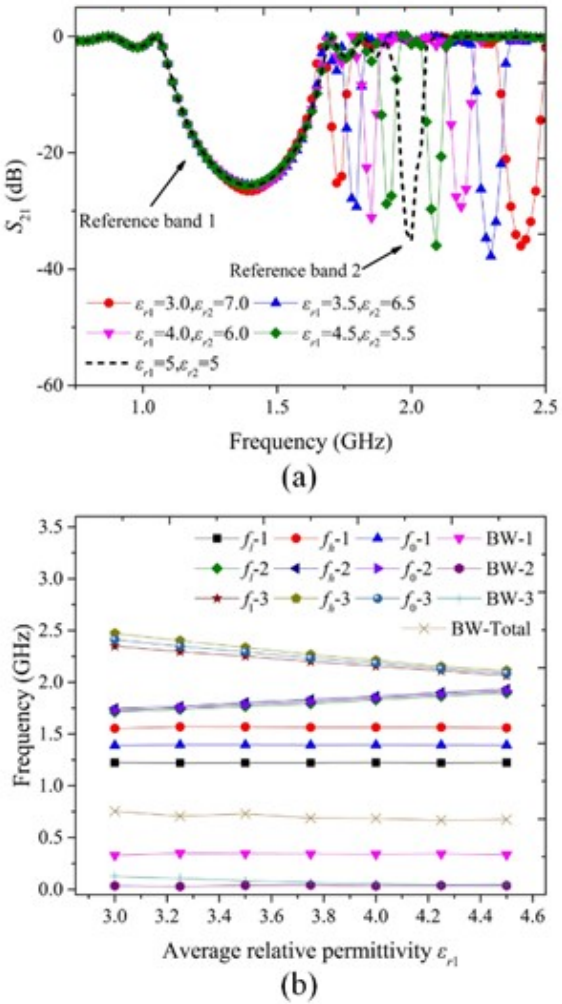

Fig. 15. Effect of ε_{r2} and ε_{r2} on transmission characteristics when $\varepsilon_r' = 5$. (a) S_{21} parameter. (b) Central frequency and bandwidth.

The effect of ε_r' on the transmission characteristics when $\varepsilon_{r1} \neq \varepsilon_{r2}$ is shown in Fig. 13. It can be seen that the EBG structure exhibits the triple-band characteristic when the dielectric parameters in grooves are different. Moreover, the exchange of the left and right dielectric parameters does not affect the transmission characteristics. As ε_r' increases, the central frequency of the first bandgap remains unchanged while the second and third bandgaps become lower.

Figure 14 shows the effect of ε_r' by adjusting ε_{r2} on the transmission characteristics when $\varepsilon_{r1} = 3.5$. As ε_{r2} increases from 4.0 to 6.5, ε_r' increases, the central frequency, and bandwidth of the first and third bandgaps

remain practically unchanged, the central frequency of the second bandgap gradually becomes lower and approaches the first bandgap, and its bandwidth remains unchanged. Combining the results shown in Fig. 13 and Fig. 14, it can be seen that the increase of dielectric parameters in both grooves may cause the central frequency of the second and third bandgap both become lower, and the increase of one-side dielectric parameter only affects the central frequency of the second bandgap.

The influence of simultaneous change in ε_{r1} and ε_{r2} on transmission characteristics when $\varepsilon_r' = 5$ is shown in Fig. 15. We defined the bandgap with lower central frequency as reference bandgap 1 and the higher central frequency as reference bandgap 2 when $\varepsilon_{r1} = \varepsilon_{r2} = 5$ (the black dash line in Fig. 15). It can be seen that the EBG structure exhibits a triple-band characteristic when $\varepsilon_r' = 5$ but $\varepsilon_{r1} \neq \varepsilon_{r2}$, the second and third bandgaps are distributed on both sides of the reference band 2. Meanwhile, the closer the values of ε_{r1} and ε_{r2} are, the closer the second and third bandgaps are to the reference bandgap 2, and the narrower the bandwidth of the third bandgap is.

The influence of electromagnetic parameters on transmission characteristics of the composite H-pillar EBG structure is analyzed by changing the average relative permittivity ε_r'. First of all, for the dual-band situation with $\varepsilon_{r1} = \varepsilon_{r2}$, the increase of ε_r' has little effect on the first bandgap but causes the central frequency of the second bandgap obviously becomes lower. Secondly, for the triple-band situation when $\varepsilon_{r1} \neq \varepsilon_{r2}$, the increase of ε_r' caused by the simultaneous increase of ε_{r1} and ε_{r2} causes the central frequency of the second and third bandgaps to decrease, the increase of the dielectric parameter on one side (ε_{r1}orε_{r2}) only causes the central frequency of the second band becomes lower. Finally, when the second bandgap of the EBG structure with $\varepsilon_r' = \varepsilon_{r1} = \varepsilon_{r2} = 5$ is defined as the reference band, as the value of ε_{r1} and ε_{r2} change simultaneously and get closer but ε_r' remains unchanged, the second and third bandgaps are distributed on both sides of the reference band but become closer to it.

In conclusion, the composite H-pillar EBG structure can effectively save metal materials on the basis of satisfying the design requirements. By adjusting the geometric and electromagnetic parameters, the EBG structure can exhibit dual- or triple-band characteristics while maintaining the characteristics of the first bandgap constant. The central frequency of the second and third bandgaps are adjustable, which increases the total bandgap width of the EBG structure and can prevent the propagation of electromagnetic waves in multiple frequency ranges.

V. CONCLUSION

In this paper, the transmission characteristics of a dielectric square-pillar EBG structure and a composite H-pillar EBG structure are analyzed. The Floquet theorem is combined with the SSMF-FETD method to simulate the periodically arranged 2-D pillar-array EBG structures while the subgridding technique and the periodicity of the EBG structure are used to reduce the calculation. The influence of geometric and electromagnetic parameters on EBG structures with different cross-section shapes and materials are compared in detail through the transmission coefficient and S_{21} parameters. From the analysis of geometric parameters, it is verified that the optimal filling ratio of the dielectric square-pillar EBG structure is 0.5, and the composite H-pillar EBG structure is effective in saving metal materials while satisfying the design requirements and exhibits dual- or triple-bandgap characteristic. The analysis of the electromagnetic parameters leads to the conclusion that the central frequency of the bandgap decreases as the average relative permittivity increases, the changes are more obvious in the high-frequency bandgaps of the composite H-pillar EBG structure. The electromagnetic parameters are also the factors that affect the number of bandgaps. The EBG structure exhibits triple-bandgap characteristics when the dielectric parameters on both grooves are different. The change of one-side dielectric parameter only affects the central frequency of the second bandgap, but for both sides, the central frequency and bandwidth of the second and third bandgaps are affected simultaneously. The work of this paper can provide references for the design and development of EBG structures.

REFERENCES

[1] A. Pirhadi, H. Bahrami, and A. Mallahzadeh, "Electromagnetic band gap (EBG) superstrate resonator antenna design for monopulse radiation pattern," *Applied Computational Electromagnetics Society (ACES) Journal*, vol. 27, no. 11, pp. 908-917, Nov. 2012.

[2] S. D. Assimonis, T. M. Kollatou, T. V. Yioultsis, and C. S. Antonopoulos, "Absorbing surfaces using EBG structures," *IEEE Trans. Magn.*, vol. 50, no. 2, pp. 197-200, Feb. 2014.

[3] M. Kim, "A compact EBG structure with wideband power/ground noise suppression using meander-perforated plane," *IEEE Trans. Electromag. Compat.*, vol. 57, no. 3, pp. 595-598, Jun. 2015.

[4] N Yang, Z. N. Chen, Y. Y. Wang, and M. Y. W. Chia. "A two-layer compact electromagnetic bandgap (EBG) structure and its applications in microstrip filter design," *Microw. Opt. Technol. Lett.*, vol. 37, no. 1, pp. 62-64, Apr. 2003.

[5] M. Y. Koledintseva, S. Radu, and J. Nuebel, "EBG common-mode 20-GHz microstrip and stripline filters: sensitivity to design parameters," *IEEE Trans. Electromag. Compat.*, vol. 62, no. 5, pp. 1989-2001, Oct. 2020.

[6] J. Y. Lee, S. H. Kim, and J. H. Jang, "Reduction of mutual coupling in planar multiple antenna by using 1-D EBG and SRR structures," *IEEE Trans. Antennas Propag.*, vol. 63, no. 9, pp. 4194-4198, Sep. 2015.

[7] H. H. Park, "Reduction of electromagnetic noise coupling to antennas in metal-framed smartphones using ferrite sheets and multi-via EBG structures," *IEEE Trans. Electromag. Compat.*, vol. 60, no. 2, pp. 394-401, Apr. 2018.

[8] P. Bora, P. Pardhasaradhi, and B. Madhav. "Design and analysis of EBG antenna for Wi-Fi, LTE, and WLAN applications," *Applied Computational Electromagnetics Society (ACES) Journal*, vol. 35, no. 9, pp. 1030-1036, Sep. 2020.

[9] W. Q. Cao, B. N. Zhang, A. J. Liu, T. B. Yu, D. S. Guo, and X. F. Pan, "Multi-frequency and dual-mode patch antenna based on electromagnetic band-gap (EBG) structure," *IEEE Trans. Antennas Propag.*, vol. 60, no. 12, pp. 6007-6012, Aug. 2012.

[10] L. Peng, C. L. Ruan, and J. Xiong, "Compact EBG for multi-band applications," *IEEE Trans. Antennas Propag.*, vol. 60, no. 9, pp. 4440-4444, Sep. 2012.

[11] V. Radisic and Y. Qian, "Broad-band power amplifier using dielectric photonic bandgap structure," *IEEE Microw. Guided Wave Lett.*, vol. 8, no. 1, pp. 13-14, Jan. 1998.

[12] Y. J. Lee, J. Yeo, R. Mittra, and W. S. Park, "Design of a high-directivity Electromagnetic band gap (EBG) resonator antenna using a frequency-selective surface (FSS) superstrate," *Microw. Opt. Technol. Lett.*, vol. 43, no. 6, pp. 462-467, Dec. 2004.

[13] A. R. Weily, K. P. Esselle, T. S. Bird, and B. C. Sanders, "Linear array of woodpile EBG sectoral horn antennas," *IEEE Trans. Antennas Propag.*, vol. 54, no. 8, pp. 2263-2274, Aug. 2006.

[14] Y. F. Mao, B. Chen, R. Xiong, Z. Cai, and Q. Chen, "A novel weakly conditionally stable FDTD method for periodic structures," *IEEE Antennas Wireless Propag. Lett.*, vol. 11, pp. 164-167, Feb. 2012.

[15] F. Yang and Y. Rahmat-Samii, "Microstrip antennas integrated with electromagnetic band-gap (EBG) structures: a low mutual coupling design for array applications," *IEEE Trans. Antennas Propag.*, vol. 51, no. 10, pp. 2936-2946, Oct. 2003.

[16] S. D. Assimonis, T. V. Yioultsis, and C. S. Antonopoulos, "Computational investigation and design of planar EBG structures for coupling reduction in antenna applications," *IEEE Trans. Magn.*, vol. 48, no. 2, pp. 771-774, Feb. 2012.

[17] M. N. Vouvakis, Z. Cendes, and J. F. Lee, "A FEM domain decomposition method for photonic and electromagnetic band gap structures," *IEEE Trans. Antennas Propag.*, vol. 54, no. 2, pp. 721-733, Feb. 2006.

[18] J. F. Lee, R. Lee, and A. Cangellaris, "Time-domain finite-element methods," *IEEE Trans. Antennas Propag.*, vol. 45, no. 3, pp. 430-442, Mar. 1997.

[19] D. Jiao and J. M. Jin, "A general approach for the stability analysis of the time-domain finite-element method for electromagnetic simulations," *IEEE Trans. Antennas Propag.*, vol. 50, no. 11, pp. 1624-1632, Nov. 2002.

[20] J. Yan and D. Jiao, "Fast explicit and unconditionally stable FDTD method for electromagnetic analysis," *IEEE Trans. Microw. Theory Tech.*, vol. 65, no. 8, pp. 2698-2710, Aug. 2017.

[21] S. H. Zhao, B Wei, X. B. He, Y. W. Li, and X. L. Wei, "Hybrid FDTD algorithm for electromagnetic analysis of fine structures," *Results Phys.,* vol. 31, pp. 105017, Dec. 2021.

[22] W. Lee and D. Jiao, "An alternative explicit and unconditionally stable time-domain finite-element method for electromagnetic analysis," *IEEE J. Multiscale Multiphys. Comput. Tech.*, vol. 3, pp. 16-28, Mar. 2018.

[23] K. H. Fan, B. Wei, and X. B. He, "A subgridding unconditionally stable FETD method based on local eigenvalue solution," *IEEE Trans. Antennas Propag*, vol. 69, no. 8, pp. 4695-4705, Aug. 2021.

[24] F. L. Teixeira, "Time-domain finite-difference and finite-element methods for Maxwell equations in complex media," *IEEE Trans. Antennas Propag.*, vol. 56, no. 8, pp. 2150-2166, Aug. 2008.

Yixin Wang was born in Xi'an, Shaanxi, China, in 1995. She received her B.S. degree in Electromagnetic Wave Propagation And Antennas from Xidian University, Xi'an, China, in 2017. She is currently pursuing a Ph.D. degree in Radio Science at the School of Physics, Xidian University. Her current research interests include the finite element time-domain method and its related methods.

Bing Wei was born in Tianshui, Gansu, China, in 1970. He received a B.S. degree in Physics from Beijing Normal University, Beijing, China, in 1993, and a Ph.D. degree in Radio Science from Xidian University, Xi'an, China, in 2004. From 1993 to 1998, he was a Physics professor at Tianshui Normal University, Tianshui, China. From 1998 to 1999, he was a Physics professor at Baoji University of Arts and Science, Baoji, China. Since 2004, he was been with Xidian University. Currently, he is also a professor at Xidian University. His research interests include investigations of electromagnetic field theory, numerical field computation, and short pulse interactions on complex objects.

Kaihang Fan was born in Linfen, Shanxi, China, in 1990. She received a B.S. degree in Electronic Information Science And Technology and a Ph.D. degree in Radio Science from Xidian University, Xi'an, China, in 2014 and 2021, respectively. She is currently working as a postdoctoral researcher at the School of Information and Communications Engineering, Xi'an Jiaotong University, Xi'an, China. Her current research interests include the finite element time-domain method and the multiphysics problem.